Nonlinear Model Predictive Control for Dynamic Operation of an Alkaline Electrolyzer

Anders Hilmar Damm Christensen * **Nicola Cantisani** *
Shi You ** **John Bagterp Jørgensen** *

* *Department of Applied Mathematics and Computer Science, Technical University of Denmark, DK-2800 Kgs. Lyngby, Denmark.*
** *Department of Wind and Energy Systems, Technical University of Denmark, DK-2800 Kgs. Lyngby, Denmark*

Abstract: This paper demonstrates how incorporating future input power information impacts the performance of a nonlinear model predictive control (NMPC) algorithm for an alkaline electrolyzer (AEL) plant. The primary objective of the NMPC is to maintain the stack temperature and number of moles of water in the AEL within operating limits, despite large variations in the input power. The NMPC combines an optimal control problem (OCP) with a continuous-discrete extended Kalman filter (CD-EKF). For both the OCP and the CD-EKF, we use a model that is different from the AEL simulation model. We present three closed-loop simulations: two where the NMPC operates at different stack temperature and water mole setpoints with only current input power information, and one where it receives information about future power changes in advance. The results show a 1.583% increase in hydrogen production when the NMPC utilizes information about future power changes.

Keywords: Power-to-X, Alkaline electrolysis, NMPC, Anticipatory control, temperature control.

1. INTRODUCTION

The green transition involves replacing fossil fuels with renewable energy sources like solar and wind. While renewables can sometimes directly substitute fossil fuels, this approach may not be feasible for sectors like heavy transport, such as buses, trucks, and large ships. In these cases, green fuels like green hydrogen and green ammonia provide viable alternatives. Power-to-X (PtX) technologies enable the conversion of excess renewable energy into such fuels. Unlike traditional chemical plants that operate optimally at steady state, PtX facilities need to be operated dynamically to handle the intermitting nature of wind and solar energy (Cantisani et al., 2023b; Sorrenti et al., 2022).

An energy management system (EMS) that uses forecasted wind and solar data is essential for the dynamic operation of PtX plants (Klyapovskiy et al., 2021). As illustrated in Fig. 1, an EMS may allocate the surplus renewable energy to a power-to-ammonia (PtA) system, determining how energy is distributed across the individual subsystems.

Since ammonia is composed of hydrogen and nitrogen, efficient hydrogen production plays a key role in a PtA plant. In addition, standalone power-to-hydrogen (PtH) plants are also recognized as important. Alkaline water electrolysis is the most mature process for hydrogen production using renewable electricity (Lingkang et al., 2023). The efficiency of an alkaline electrolyzer (AEL) plant depends on the temperature of the liquid alkaline electrolyte solution (Øystein Ulleberg, 2003; Qi et al., 2023). Higher temperatures improve efficiency and enable more hydrogen production from the same power input. However, excessive heat can degrade the system. Operating at a lower temperature allows the EMS to supply higher power inputs to the AEL, increasing hydrogen production by utilizing this additional energy. However, this comes at the cost of slightly lower efficiency due to the reduced temperature.

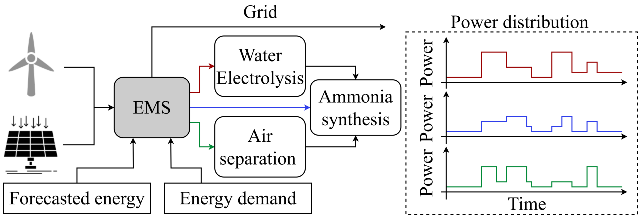

Fig. 1. Sketch: The EMS allocates forecasted excess renewable energy to individual subsystems.

An anticipatory control system is advantageous when operating an AEL close to its maximum temperature while handling large changes in input power. While temperature stabilization using proportional-integral-derivative (PID)-type control has been demonstrated for AEL systems (Qi et al., 2023; Huang et al., 2023), model predictive control (MPC) can optimize system dynamics under constraints. When disturbances can be anticipated, an MPC algorithm can proactively control the system to maintain efficiency while respecting these constraints. MPC has been applied to AEL plants in previous studies: Qi et al. (2023) compares PID control with MPC, showing that MPC reduces

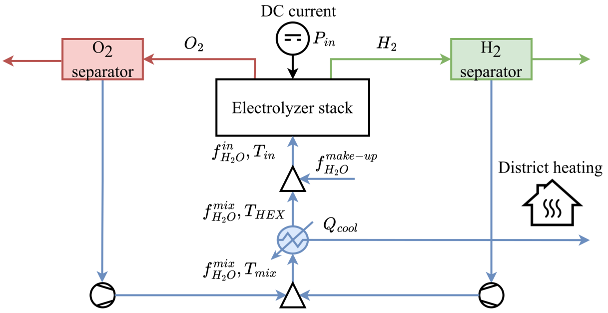

Fig. 2. Schematic diagram of the AEL plant.

temperature fluctuations by anticipating power changes, while Qiu et al. (2024) applies nonlinear MPC (NMPC) for grid-connected PtH load-tracking, demonstrating its ability to reduce hydrogen-to-oxygen impurity accumulation. However, no studies have directly demonstrated the impact on NMPC performance for an AEL plant when using future input power information, compared to relying solely on current power data.

This paper presents an NMPC algorithm for temperature stabilization in an AEL subjected to system constraints. By using a known input power sequence, the NMPC increases hydrogen production while maintaining these system constraints, as compared to when only current power data is available. We demonstrate this through three closed-loop simulations: two simulations use only current power information at different temperature set-points, while the third incorporates future power changes. Our results show that anticipating power changes increases hydrogen production.

The rest of the paper is organized as follows: Section 2 summarizes the simulation model of the AEL using a thermodynamic library. In Section 3, we present the NMPC algorithm. Section 4 shows closed-loop numerical experiments of the AEL and Section 5 presents conclusions.

2. MODELING

We model the AEL plant as a system of stochastic differential-algebraic equations (SDAEs) with discrete-time measurements of the form

$$\begin{aligned} dx(t) &= f(t, x(t), y(t), u(t), d(t))dt + \sigma d\omega(t), && \text{(1a)}\\ 0 &= g(t, x(t), y(t), u(t), d(t)), && \text{(1b)}\\ m_k &= l(t_k, x_k, y_k, u_k, d_k) + v_k, && \text{(1c)}\\ z(t) &= h(t, x(t), y(t), u(t), d(t)). && \text{(1d)} \end{aligned}$$

$f(\cdot)$ is the drift, σ are the diffusion coefficients, $g(\cdot)$ represents the algebraic equations, and $l(\cdot)$ and $h(\cdot)$ represent the measurement and output equations, respectively. $\omega(t)$ is a standard Wiener process, i.e., $d\omega(t) \sim N_{iid}(0, Idt)$ and $v_k \sim N_{iid}(0, R_k)$ is the measurement noise with R_k being the covariance. $m_k = m(t_k)$ are the measurements at the time t_k, and $z(t)$ is the output of the model.

We use the AEL model described by Cantisani et al. (2023a), with some modifications. Fig. 2 shows the schematic diagram of the AEL plant. The AEL plant consists of an electrolyzer stack, two gas/liquid separators, and a water recirculation system. The water recirculation system includes a heat exchanger to remove heat from the recirculated water, which is mixed with fresh make-up water before re-entering the stack.

We use the ThermoLib library (Ritschel et al., 2017) to evaluate the thermodynamic properties of gases and liquids in the AEL. The main unit, the electrolyzer stack, and the modifications to the model in Cantisani et al. (2023a) are presented in the following sections.

2.1 The electrolyzer stack

The electrolyzer stack splits water into hydrogen and oxygen using electrical power. The reaction is

$$\mathrm{H_2O(l)} + \text{Electrical power} \longrightarrow \mathrm{H_2(g)} + \frac{1}{2}\mathrm{O_2(g)}. \qquad (2)$$

Alkaline electrolysis technology is characterized by having two electrodes, i.e., cathode and anode., that operates in a liquid alkaline electrolyte solution of potassium hydroxide (KOH), usually 20-40%, or sodium hydroxide (NaOH), separated by a diaphragm. The electrolyzer stack consists of multiple electrolytic cells connected in series. We model the electrolyzer stack using mass and energy balances combined with an electrochemical part (Cantisani et al., 2023a). The model equations are

$$\begin{aligned} \dot{T}_{stack} &= \frac{1}{C_{P,el}}\Big(\tilde{H}_{in} - \tilde{H}_{out} + Q + W_e\Big), && \text{(3a)}\\ 0 &= U_{cell} - U_{rev}(T_{stack}), \\ &\quad - U_{ohm}(I, T_{stack}) - U_{act}(I, T_{stack}), && \text{(3b)}\\ 0 &= P_{in} - n_c U_{cell} I. && \text{(3c)} \end{aligned}$$

The differential equation (3a) describes the dynamics of the temperature, T_{stack}, in the electrolyzer, by considering its energy balance. $\tilde{H}_{in}$ and $\tilde{H}_{out}$ are the enthalpy flows in and out, Q is heat flow exchanged with the ambient (convective) and W_e is the electrical work. Specifically

$$\begin{aligned} W_e &= P_{in}, && \text{(4a)}\\ Q &= -Q_{amb} = -A_s h_c (T_{stack} - T_{amb}), && \text{(4b)}\\ \tilde{H}_{in} &= H(T_{in}, P, f^{in}_{H_2O})(l), && \text{(4c)}\\ \tilde{H}_{out} &= H(T_{stack}, P, f_{out,H_2O})(l) \\ &\quad + H(T_{stack}, P, f_{out,H_2})(g) \\ &\quad + H(T_{stack}, P, f_{out,O_2})(g). && \text{(4d)} \end{aligned}$$

A_s is the active area of heat transfer, h_c is the heat transfer coefficient, T_{amb} is the ambient temperature, and P is the pressure. Eq. (3b) describes the electrochemical model. The total cell voltage, U_{cell}, is defined by the sum of the contributions

$$U_{rev} = \frac{\Delta G_r}{z_e F} = \frac{\Delta H_r - T_{stack}\Delta S_r}{z_e F}, \qquad (5a)$$

$$U_{ohm} = (r_1 + r_2 T_{stack})\frac{I}{A}, \qquad (5b)$$

$$U_{act} = s \log\left(\left(t_1 + \frac{t_2}{T_{stack}} + \frac{t_3}{T^2_{stack}}\right)\frac{I}{A} + 1\right). \qquad (5c)$$

Eq. (3c) relates the input power, P_{in}, to the current, I, and total voltage, U_{cell}. The parameters r_1 and r_2 represent ohmic resistance, and s, and t_1, t_2, t_3 are the activation overvoltage coefficients. A is the electrode area, F is the Faraday's constant, $z_e = 2$ is the number of electrons transferred, and n_c is the number of electrolytic cells. By defining a static mass balance in the electrolyzer, the molar flow rate at the outlet can be computed as

$$f_{out} = \begin{bmatrix} f_{out,H_2O} \\ f_{out,H_2} \\ f_{out,O_2} \end{bmatrix} = \begin{bmatrix} f^{in}_{H_2O} \\ 0 \\ 0 \end{bmatrix} + \begin{bmatrix} -1 \\ 1 \\ 1/2 \end{bmatrix} r. \tag{6}$$

The reaction rate, r, is a function of the current, given by

$$r = r(I) = n_c \frac{\eta_F}{z_e F} I, \quad \eta_F = \frac{(I/A)^2}{f_1 + (I/A)^2} f_2, \tag{7}$$

where η_F is the Faraday efficiency, with f_1 and f_2 as parameters.

2.2 Peripherals and water recirculation system

The presented model differs from the model described by Cantisani et al. (2023a), by mixing the flow from the separators into a combined recirculated flow, $f^{mix}_{H_2O}$, before heat is removed using a heat exchanger. The temperature of the flow before and after the heat exchanger are T_{mix} and T_{HEX}, respectively. We model mass and energy balances in the mixing of separator outflows as the algebraic equations

$$\begin{aligned} 0 &= f^{mix}_{H_2O} - f^{sep,1}_{H_2O} - f^{sep,2}_{H_2O}, && \text{(8a)} \\ 0 &= H(T_{mix}, P, f^{mix}_{H_2O}) \\ &\quad - H(T_{sep,1}, P, f^{sep,1}_{H_2O}) - H(T_{sep,2}, P, f^{sep,2}_{H_2O}). && \text{(8b)} \end{aligned}$$

The static heat exchanger is modeled as

$$0 = H(T_{mix}, P, f^{mix}_{H_2O}) - H(T_{HEX}, P, f^{mix}_{H_2O}) - Q_{cool}. \tag{9}$$

Finally, we model the mixing of make-up water with the recirculated water as

$$\begin{aligned} 0 &= f^{in}_{H_2O} - f^{mix}_{H_2O} - f^{make-up}_{H_2O}, && \text{(10a)} \\ 0 &= H(T_{in}, P, f^{in}_{H_2O}) - H(T_{mix}, P, f^{mix}_{H_2O}) \\ &\quad - H(T_{make-up}, P, f^{make-up}_{H_2O}). && \text{(10b)} \end{aligned}$$

$f^{in}_{H_2O}$ and T_{in} are the flow and temperature of the water entering the electrolyzer stack. This flow is a combination of the recirculated flow and make-up water, $f^{make-up}_{H_2O}$, at temperature $T_{make-up}$.

The gas-liquid separators are modeled exactly as in (Cantisani et al., 2023a) (mass and energy balances). We indicate with $n^{sep,1}_{H_2O}$, $n^{sep,1}_{O_2}$, $U_{sep,1}$, $T_{sep,1}$, $P_{sep,1}$ the number of moles of water and oxygen, the internal energy, the temperature and the pressure in separator 1, respectively. $n^{sep,2}_{H_2O}$, $n^{sep,2}_{H_2}$, $T_{sep,2}$, $P_{sep,2}$ and $U_{sep,2}$ are the number of moles of water and hydrogen, the temperature, the pressure and internal energy in separator 2, respectively.

Low-level controllers for the separators: The flows of liquids and gases out of the separators, denoted as $f^{sep,1}_{H_2O}$, $f^{sep,2}_{H_2O}$, $f^{sep,1}_{O_2}$, and $f^{sep,2}_{H_2}$, are manipulated variables (MVs). To simplify the design of the NMPC, these MVs are modeled as low-level P-controllers (LLCs) of the form

$$f^{LLC}_{out} = \bar{f}^{LLC}_{out} + K_p(n - \bar{n}), \tag{11}$$

where f^{LLC}_{out} represents a flow of material out of a separator, with n being the controlled variable. $\bar{f}^{LLC}_{out}$ and $\bar{n}$ represent MV operating point and setpoint, respectively. These controllers stabilize the separators for a given inlet gas/liquid flow. As a result, the MVs are no longer directly controlled by the NMPC, but this also means that the moles of water in the separators cannot be controlled independently.

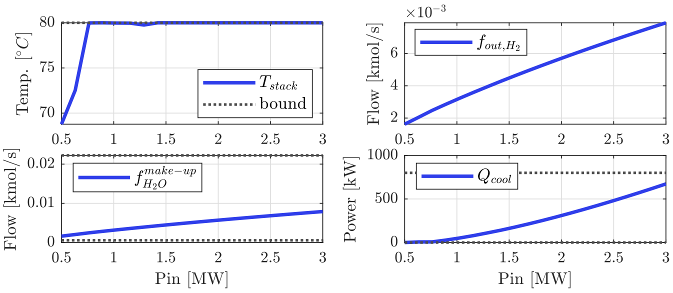

Fig. 3. Steady state optimization of the AEL across a range of inlet power levels.

2.3 Plant-wide model

We obtain the complete plant-wide model by combining the differential and algebraic equations of each component. This results in the differential variables

$$\begin{aligned} x(t) = [&T_{stack}, n^{sep,1}_{H_2O}, n^{sep,1}_{O_2}, U_{sep,1}, n^{sep,2}_{H_2O}, \\ &n^{sep,2}_{H_2}, U_{sep,2}]^T. \end{aligned} \tag{12}$$

The algebraic variables are

$$\begin{aligned} y(t) = [&U_{cell}, I, T_{sep,1}, P_{sep,1}, T_{sep,2}, P_{sep,2}, f^{mix}_{H_2O}, \\ &T_{mix}, T_{HEX}, f^{in}_{H_2O}, T_{in}]^T. \end{aligned} \tag{13}$$

The MVs left for the NMPC to use are the flow of make-up water and the energy removal in the heat exchanger,

$$u(t) = [f^{make-up}_{H_2O}, Q_{cool}]^T. \tag{14}$$

Finally, the disturbances are the ambient temperature, the input power to the electrolyzer stack, and the temperature of the make-up water, i.e.,

$$d(t) = [T_{amb}, P_{in}, T_{make-up}]^T. \tag{15}$$

2.4 Steady state optimization

We find the operating conditions that maximize hydrogen production by solving steady state optimization problems of the form

$$\begin{aligned} \max_{x_s, y_s, u_s} \quad & f_{out,H_2} = r(I), && \text{(16a)} \\ s.t. \quad & 0 = f(t_{ss}, x_{ss}, y_{ss}, u_{ss}, d_i), && \text{(16b)} \\ & 0 = g(t_{ss}, x_{ss}, y_{ss}, u_{ss}, d_i), && \text{(16c)} \\ & x_{min} \le x_{ss} \le x_{max}, && \text{(16d)} \\ & u_{min} \le u_{ss} \le u_{max}. && \text{(16e)} \end{aligned}$$

In these problems, we gradually increase the input power to the AEL. We assume a maximum allowed stack temperature of 80°C and we impose bounds on the MVs. The disturbances d_i include $[T_{amb}, P_{in,i}, T_{make-up}]$, where $P_{in,i}$ is swept from 0.5 MW to 3.0 MW. Fig. 3 shows that the optimal steady state solutions are at the maximum allowed temperature of 80°C. However, at lower power levels, this temperature cannot be maintained at a steady state.

3. NONLINEAR MODEL PREDICTIVE CONTROL

We present an NMPC strategy for tracking a temperature setpoint in the stack and maintaining a setpoint for the number of moles of water in separator 2. The NMPC also incorporates soft bounds on the stack temperature and the moles of water in both separators, with additional penalties applied to the rate of movement of the MVs. The NMPC combines a continuous-discrete extended Kalman filter (CD-EKF) with an optimal control problem (OCP) to compute a control signal after each measurement, which is then applied to the plant before the next measurement is taken. We assume that the disturbance vector remains piecewise constant between measurements. A zero-order-hold parameterization is applied, i.e., $u(t) = u_k$, $d(t) = d_k$, for $t \in [t_k, t_{k+1}]$, where the sampling time is $T_s = t_{k+1} - t_k$ and u_k represents the implemented control signal computed by the OCP at time t_k.

3.1 Simplified control model for the NMPC

We present a simplified control model for NMPC, that approximates the temperature dynamics in the electrolyzer without using ThermoLib. This model uses constant heat capacities and basic energy balances, similar to the models presented by Øystein Ulleberg (2003). In this model, we formulate the separator temperatures, $T_{sep,1}$ and $T_{sep,2}$, as differential states instead of algebraic variables and extend the disturbance vector for this model with the additional disturbances,

$$\begin{aligned} d_{ext}(t) = [d(t)^T, d_{add}(t)^T]^T = [&T_{amb}, P_{in}, T_{make-up}, \\ &T_{stack,d}, n^{sep,1}_{H_2O,d}, n^{sep,2}_{H_2O,d}, \\ &T_{sep,1,d}, T_{sep,2,d}]^T, \end{aligned} \tag{17}$$

to represent plant-model mismatch in the differential equations. The simplified model is a system of DAEs of the form

$$\dot{x}^c(t) = f^c(t, x^c(t), y^c(t), u(t), d_{ext}(t)), \tag{18a}$$

$$0 = g^c(t, x^c(t), y^c(t), u(t), d_{ext}(t)). \tag{18b}$$

The differential state vector of (18) is

$$x^c(t) = [T_{stack}, n^{sep,1}_{H_2O}, n^{sep,2}_{H_2O}, T_{sep,1}, T_{sep,2}]^T, \tag{19}$$

and we model (18a) as

$$\dot{T}_{stack} = \frac{1}{C_{P,el}}\left(Q_{gen} + Q_{liq} - Q_{amb}\right), \tag{20a}$$

$$\dot{n}^{sep,1}_{H_2O} = f^{sep,1}_{in,H_2O} - f^{sep,1}_{H_2O} + n^{sep,1}_{H_2O,d}, \tag{20b}$$

$$\dot{n}^{sep,2}_{H_2O} = f^{sep,2}_{in,H_2O} - f^{sep,2}_{H_2O} + n^{sep,2}_{H_2O,d}, \tag{20c}$$

$$\dot{T}_{sep,1} = f^{sep,1}_{in,H_2O}\frac{T_{stack} - T_{sep,1}}{n^{sep,1}_{H_2O}} + T_{sep,1,d}, \tag{20d}$$

$$\dot{T}_{sep,2} = f^{sep,2}_{in,H_2O}\frac{T_{stack} - T_{sep,2}}{n^{sep,2}_{H_2O}} + T_{sep,2,d}, \tag{20e}$$

with

$$Q_{liq} = f^{in}_{H_2O} c_{p,lye}(T_{in} - (T_{stack} + T_{stack,d})), \tag{21a}$$

$$Q_{gen} = n_c(U_{cell} - U_{tn})I, \tag{21b}$$

$$f^{sep,1}_{in,H_2O} = f^{in}_{H_2O}/2 + r(I), \tag{21c}$$

$$f^{sep,2}_{in,H_2O} = f^{in}_{H_2O}/2 - 2r(I). \tag{21d}$$

$c_{p,lye}$ is the heat capacity of the lye and U_{tn} is the thermoneutral cell voltage (Øystein Ulleberg, 2003). The algebraic variables are

$$y^c(t) = [U_{cell}, I, f^{mix}_{H_2O}, T_{mix}, T_{HEX}, f^{in}_{H_2O}, T_{in}]^T, \tag{22}$$

and we model (18b) as

$$0 = U_{cell} - (U_{rev} + U_{ohm} + U_{act}), \tag{23a}$$

$$0 = P_{in} - n_c U_{cell} I, \tag{23b}$$

$$0 = f^{mix}_{H_2O} - f^{sep,1}_{H_2O} + f^{sep,2}_{H_2O}, \tag{23c}$$

$$\begin{aligned} 0 = {} & T_{mix} f^{mix}_{H_2O} c_{p,lye} \\ & - c_{p,lye}(T_{sep,1} f^{sep,1}_{H_2O} + T_{sep,2} f^{sep,2}_{H_2O}), \end{aligned} \tag{23d}$$

$$0 = T_{HEX} - (T_{mix} - \frac{Q_{cool}}{f^{mix}_{H_2O} c_{p,lye}}), \tag{23e}$$

$$0 = f^{in}_{H_2O} - (f^{mix}_{H_2O} + f^{make-up}_{H_2O}), \tag{23f}$$

$$\begin{aligned} 0 = {} & f^{in}_{H_2O} T_{in} c_{p,lye} \\ & - c_{p,lye}(f^{mix}_{H_2O} T_{HEX} + f^{make-up}_{H_2O} T_{make-up}). \end{aligned} \tag{23g}$$

We distinguish the drift and algebraic terms as $f(\cdot)$, $g(\cdot)$ for the original ThermoLib model, and $f^c(\cdot)$, $g^c(\cdot)$ for the control model.

3.2 Continuous-discrete extended Kalman filter

We implement the CD-EKF similarly to the implementation in Christensen et al. (2024). Using measurements m_k and the previous control u_{k-1}, the CD-EKF computes filtered differential and algebraic states, $\hat{x}^c_{k|k}$, $\hat{y}^c_{k|k}$, and state covariance $P_{k|k}$ at time t_k. The filtered differential state vector is used as the initial conditions for the OCP. The initial states and covariance are $\hat{x}^c_{0|-1} = x_0$, $\hat{y}^c_{0|-1} = y_0$, and $P_{0|-1} = P_0$, respectively.

Filtering: We compute the innovation, e_k, as

$$e_k = m_k - \hat{m}_{k|k-1}, \tag{24}$$

using the estimated measurement at time t_k

$$\hat{m}_{k|k-1} = l(t_k, \hat{x}^c_{k|k-1}, \hat{y}^c_{k|k-1}, u_{k-1}, d_k). \tag{25}$$

The covariance of the innovation, $R_{e,k}$, is computed as

$$R_{e,k} = C_k P_{k|k-1} C_k^T + R_k, \tag{26a}$$

$$C_k = \frac{\partial l_{k|k-1}}{\partial x^c} + \frac{\partial l_{k|k-1}}{\partial y^c}\frac{\partial \hat{y}^c_{k|k-1}}{\partial x^c}. \tag{26b}$$

with R_k being the measurement noise covariance. The sensitivity $\frac{\partial \hat{y}^c_{k|k-1}}{\partial x^c}$ is calculated by solving

$$\frac{\partial g_{k|k-1}}{\partial y^c}\frac{\partial y^c_{k|k-1}}{\partial x^c} = -\frac{\partial g_{k|k-1}}{\partial x^c}, \tag{27}$$

where

$$l_{k|k-1} = l(t_k, \hat{x}^c_{k|k-1}, \hat{y}^c_{k|k-1}, u_{k-1}, d_k), \tag{28a}$$

$$g_{k|k-1} = g^c(t_k, \hat{x}^c_{k|k-1}, \hat{y}^c_{k|k-1}, u_{k-1}, d_k). \tag{28b}$$

We compute the Kalman gain and the filtered state as

$$K_k = P_{k|k-1} C_k^T R_{e,k}^{-1}, \quad \hat{x}^c_{k|k} = \hat{x}^c_{k|k-1} + K_k e_k, \tag{29}$$

respectively. The filtered covariance is calculated as

$$P_{k|k} = (I - K_k C_k) P_{k|k-1} (I - K_k C_k)^T + K_k R_k K_k^T, \tag{30}$$

and we compute the algebraic state, $\hat{y}_{k|k}$, by solving

$$0 = g^c(t_k, \hat{x}^c_{k|k}, \hat{y}^c_{k|k}, u_{k-1}, d_k). \tag{31}$$

Prediction: We compute one-step predictions, $\hat{x}^c_{k+1|k} = \hat{x}^c_k(t_{k+1})$ and $\hat{y}^c_{k+1|k} = \hat{y}^c_k(t_{k+1})$, by solving

$$\frac{d\hat{x}_k(t)}{dt} = f^c(\hat{x}^c_k(t), \hat{y}^c_k(t), u_k, d_k), \tag{32a}$$

$$0 = g^c(\hat{x}^c_k(t), \hat{y}^c_k(t), u_k, d_k), \tag{32b}$$

for $t \in [t_k,\, t_{k+1}]$, with initial conditions $\hat{x}_k^c(t_k) = \hat{x}_{k|k}^c$ and $\hat{y}_k^c(t_k) = \hat{y}_{k|k}^c$ using an implicit Euler integration scheme. We compute the predicted differential state covariance, $P_{k+1|k} = P_k(t_{k+1})$, as the solution to

$$\begin{aligned} P_k(t) &= \Phi_{xx}(t,t_k)P_k(t_k)\Phi_{xx}^T(t,t_k) \\ &\quad + \int_{t_k}^{t} \Phi_{xx}(t,s)\sigma\sigma^T\Phi_{xx}(t,s)ds, \end{aligned} \tag{33}$$

at time $t = t_{k+1}$, with the initial condition $P_k(t_k) = P_{k|k}$ (Jørgensen et al., 2007). $\Phi_{xx}(t,s) = \frac{\partial \hat{x}_k^c(t)}{\partial \hat{x}_k^c(s)}$ is the differential state sensitivity which we calculate using a staggered direct approach.

Disturbance augmentation: To achieve offset-free control, we extend $f^c(\cdot)$ with integrating disturbance models in the CD-EKF, such that an estimate of $d_{add}(t)$ can be computed. We model the dynamics of the additional disturbances as the system of stochastic differential equations (SDEs) of the form

$$dd_{add,i}(t) = \sigma_{d,i}d\omega_{d,i}(t), \quad i \in \{1,2,3,4,5\}, \tag{34}$$

with $\sigma_{d,i}$ being tuning parameters for the CD-EKF.

3.3 Optimal control problem

We formulate an optimal control problem (OCP) that penalizes tracking errors in the electrolyzer stack temperature and the number of moles of water in separator 2, $z(t) - \bar{z}(t)$, as well as the input rate of movement, $\Delta u_k = u_k - u_{k-1}$, using a least-squares approach. The OCP also includes bounds on the separators and the temperature of the stack. We solve the OCP at time t_k with prediction horizon T_N using the filtered differential state, $\hat{x}_{k|k}^c$ and disturbances $\hat{d}_{add,k|k}$, as initial conditions. We divide the control horizon, $[t_k,\, t_k + T_N]$, into $N = T_N/T_s$ equally spaced subintervals, $[t_{k+j},\, t_{k+j+1}]$, with $j \in \mathcal{N} = 1, \ldots, N-1$. The OCP is

$$\min_{x,y,u} \quad \phi_k = \phi_{cont} + \phi_{\Delta u,k}, \tag{35a}$$

$$s.t. \quad x^c(t_k) = \hat{x}_{k|k}^c, \tag{35b}$$

$$d_{add}(t_k) = \hat{d}_{add,k|k}, \tag{35c}$$

$$\dot{x}^c(t) = f^c(t, x^c, y^c, u, d_{ext}),\ t \in [t_k,\, t_k + T_N], \tag{35d}$$

$$0 = g^c(t, x^c, y^c, u, d_{ext}),\ t \in [t_k,\, t_k + T_N], \tag{35e}$$

$$u(t) = u_{k+j},\ t \in [t_{k+j},\, t_{k+j+1}],\ j \in \mathcal{N}, \tag{35f}$$

$$d(t) = d_{k+j},\ t \in [t_{k+j},\, t_{k+j+1}],\ j \in \mathcal{N}, \tag{35g}$$

$$u_{\min} \le u_{k+j} \le u_{\max}, j \in \mathcal{N}, \tag{35h}$$

where $\phi_{\Delta u,k}$ is described as

$$\phi_{\Delta u,k} = \frac{1}{2}\sum_{j=0}^{N-1} \|\Delta u_{k+j}\|_{\bar{Q}_{\Delta u}}^2, \quad \bar{Q}_{\Delta u} = Q_{\Delta u}/T_s, \tag{36}$$

and ϕ_{cont} represent the continuous objectives of the form

$$\phi_{cont} = \int_{t_k}^{t_k+T_N} \phi_z(T_{stack}) + \phi_z(n_{H2O}^{sep,1}) + \phi_z(n_{H2O}^{sep,2})dt. \tag{37}$$

We define $\phi_z(z)$ as

$$\begin{aligned} \phi_z(z) &= \alpha_{\bar{z}}\frac{1}{2}(z - \bar{z})^2 + \alpha_{z_{bounds}}\min(0, z - z_{min})^2 \\ &\quad + \alpha_{z_{bounds}}\min(0, -z + z_{max})^2, \end{aligned} \tag{38}$$

where $\alpha_{\bar{z}}$ and $\alpha_{z_{bounds}}$ are the tuning parameters. As a result, we have two tuning parameters for each of the three terms in (37), i.e, $(\alpha_{\bar{z}}^{T_{stack}}, \alpha_{z_{bounds}}^{T_{stack}})$, $(\alpha_{\bar{z}}^{n_{H2O}^{sep,1}}, \alpha_{z_{bounds}}^{n_{H2O}^{sep,1}})$, and $(\alpha_{\bar{z}}^{n_{H2O}^{sep,2}}, \alpha_{z_{bounds}}^{n_{H2O}^{sep,2}})$. We apply a direct multiple shooting discretization scheme to transcribe (35)-(38) into a nonlinear programming (NLP) problem using an explicit singly diagonal implicit Runge-Kutta 34 (ESDIRK34) integration scheme with 5 integration steps and sensitivity computation using an iterated internal numerical differentiation approach similarly to the implementation in Christensen et al. (2024). We solve the NLP using IPOPT (Wächter and Biegler, 2006).

4. NUMERICAL EXPERIMENTS

This section presents three closed-loop simulations: in the first two, the NMPC uses only current input power information, while in the third, it receives future power changes 4 hours in advance ($T_N = 4$ h). We apply soft bounds of 60°C $\le T_{\text{stack}} \le$ 78°C and 2 kmol $\le n_{H_2O}^{\text{sep},i} \le$ 90 kmol for $i = 1, 2$. For simulations 1 and 3, we apply nominal setpoints of 75°C for the stack temperature and 45 kmol for separator 2. In simulation 2, these setpoints are adjusted to 64°C and 20 kmol to accommodate large sudden temperature increases caused by fluctuations in input power. The MVs are constrained by $0 \le f_{H_2O}^{\text{make-up}} \le 2.5$ kg/s and $0 \le Q_{\text{cool}} \le 800$ kW. The objectives are tuned with $Q_{\Delta u} = \text{diag}([10, 0.01])$, and weights $(\alpha_{\bar{z}}^{T_{\text{stack}}}, \alpha_{z_{\text{bounds}}}^{T_{\text{stack}}}) = (10.0, 100.0)$, $(\alpha_{\bar{z}}^{n_{H_2O}^{\text{sep},1}}, \alpha_{z_{\text{bounds}}}^{n_{H_2O}^{\text{sep},1}}) = (0.0, 10.0)$, and $(\alpha_{\bar{z}}^{n_{H_2O}^{\text{sep},2}}, \alpha_{z_{\text{bounds}}}^{n_{H_2O}^{\text{sep},2}}) = (0.1, 10.0)$. Notice that we have no weights on the tracking of moles in separator 1, as we cannot control. We simulate the SDAEs (1) over a 14-hour timespan using an implicit-explicit integration method, with the diffusion term $\sigma = \text{diag}([0.2, 0, \ldots, 0])$ and we measure $x^c(t)$ with measurement noise covariance $R_k = \text{diag}([0.01, 0.001, 0.001, 0.01, 0.01])$. The sampling time of the NMPC is chosen as $T_s = 5$ min. In all three simulations, we apply a power sequence that, without anticipatory control or low-temperature operation, would drive the stack temperature above 80°C.

Results and Discussion: Fig. 4 shows the results of the closed-loop simulations. The NMPCs using only current power information are labeled 'w/o prev.' (without preview), while the one with knowledge about future power changes is labeled 'w/ prev.' (with preview). Table 1 presents the total hydrogen produced in the simulations.

The results show that the NMPC with knowledge of future power changes, cools the stack in advance to handle the large power increase. When Qcool is limited, the NMPC uses $f_{H_2O}^{\text{make-up}}$ for additional cooling. However, increasing this MV fills the separators, so the NMPC proactively reduces the number of moles in the separators to extend the cooling duration of $f_{H_2O}^{\text{make-up}}$. As a result, the NMPC with future power information operates closer to the temperature limit compared to the NMPC using only current power data. From Table 1, we observe that the NMPC with future power information (w/ prev.) increases hydrogen production by 1.583% compared to the NMPC without future power information (w/o prev.) in

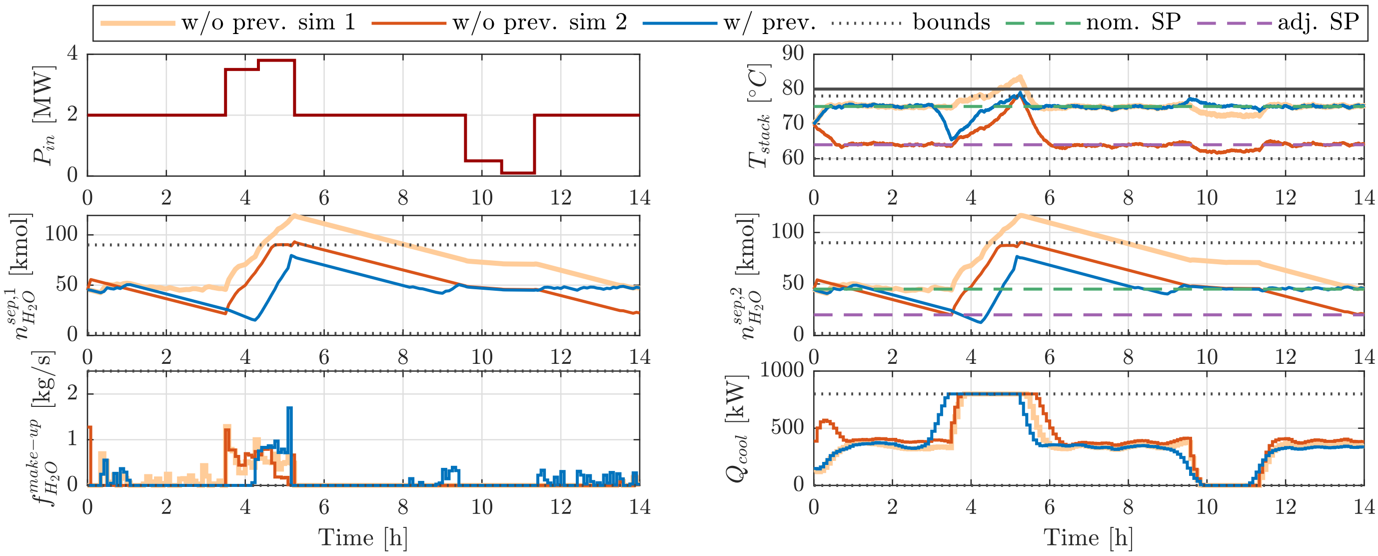

Fig. 4. Three closed-loop simulations of the NMPC applied to the AEL plant.

Table 1. Hydrogen production from the closed-loop simulations in Fig. 4.

NMPC	w/o prev. sim 1	w/o prev. sim 2	w/ prev.
H_2 produced	559.26 kg	549.30 kg	558.00 kg

simulation 2. In simulation 1, the NMPC without future power information produces more hydrogen due to a higher average temperature, but this exceeds the temperature limit, making it unviable.

5. CONCLUSIONS

This paper presents closed-loop simulations of an NMPC for temperature and mole tracking in an AEL plant. Three simulations are performed: the first two use only current input power information, while the third incorporates information about future power changes. The results demonstrate that using future power information improves the hydrogen production by allowing the AEL to operate closer to the maximum allowable temperature, while effectively managing large temporary power changes.

REFERENCES

Cantisani, N., Dovits, J., and Jørgensen, J.B. (2023a). Differential algebraic modeling of an alkaline electrolyzer plant. *arXiv preprint arXiv: 2311.09882*.

Cantisani, N., Ritschel, T.K.S., Thilker, C.A., Madsen, H., and Jørgensen, J.B. (2023b). Modeling, scientific computing and optimal control for renewable energy systems with storage. In *Proceedings of 2023 European Control Conference.*

Christensen, A.H.D., Cantisani, N., and Jørgensen, J.B. (2024). ESDIRK-based nonlinear model predictive control for stochastic differential-algebraic equations. *arXiv preprint arXiv: 2407.18852*.

Huang, C., Jin, X., Zong, Y., You, S., Træholt, C., and Zheng, Y. (2023). Operational flexibility analysis of alkaline electrolyzers integrated with a temperature-stabilizing control. *Energy Reports*, 9, 16–20.

Jørgensen, J.B., Kristensen, M.R., Thomsen, P.G., and Madsen, H. (2007). New extended Kalman filter algorithms for stochastic differential algebraic equations. In R. Findeisen, F. Allgöwer, and L.T. Biegler (eds.), *Assessment and Future Directions of Nonlinear Model Predictive Control*, 359–366. Springer Berlin Heidelberg.

Klyapovskiy, S., Zheng, Y., You, S., and Bindner, H.W. (2021). Optimal operation of the hydrogen-based energy management system with P2X demand response and ammonia plant. *Applied Energy*, 304, 117559.

Lingkang, J., Nakashima, R.N., Comodi, G., and Frandsen, H.L. (2023). Alkaline electrolysis for green hydrogen production: techno-economic analysis of temperature influence and control. In *Proceedings of ECOS 2023 - The 36th International Conference on Efficiency, Cost, Optimization, Simulation and Environmental Impact of Energy Systems 2023*, 908–919.

Qi, R., Li, J., Lin, J., Song, Y., Wang, J., Cui, Q., Qiu, Y., Tang, M., and Wang, J. (2023). Thermal modeling and controller design of an alkaline electrolysis system under dynamic operating conditions. *Applied Energy*, 332, 120551.

Qiu, Y., Zhang, H., Zhou, Y., Zang, T., Zhou, B., and Chen, G. (2024). Nonlinear model predictive control of alkaline electrolyzers to provide ancillary services. In *2024 IEEE 7th International Electrical and Energy Conference (CIEEC)*, 2819–2824. Harbin, China.

Ritschel, T.K.S., Gaspar, J., and Jørgensen, J.B. (2017). A thermodynamic library for simulation and optimization of dynamic processes. *IFAC-PapersOnLine*, 50(1), 3542–3547.

Sorrenti, I., Rasmussen, T.B.H., You, S., and Wu, Q. (2022). The role of power-to-X in hybrid renewable energy systems: A comprehensive review. *Renewable and Sustainable Energy Reviews*, 165, 112380.

Wächter, A. and Biegler, L.T. (2006). On the implementation of an interior-point filter line-search algorithm for large-scale nonlinear programming. *Mathematical Programming*, 106, 25–57.

Øystein Ulleberg (2003). Modeling of advanced alkaline electrolyzers: a system simulation approach. *International Journal of Hydrogen Energy*, 28(1), 21–33.